THE JOURNAL OF BIOLOGICAL CHEMISTRY
Vol. 278, No. 25, Issue of June 20, pp. 22972–22979, 2003
Printed in U.S.A.

Impact of N-terminal Myristoylation on the Ca^{2+}-dependent Conformational Transition in Recoverin*

Received for publication, January 15, 2003, and in revised form, April 8, 2003
Published, JBC Papers in Press, April 9, 2003, DOI 10.1074/jbc.M300447200

Oliver H. Weiergräber‡, Ivan I. Senin§, Pavel P. Philippov§, Joachim Granzin‡, and Karl-Wilhelm Koch¶‖

From the ‡Institut für Biologische Informationsverarbeitung IBI-2 (Biologische Strukturforschung) and the ¶Institut für Biologische Informationsverarbeitung IBI-1, Forschungszentrum Jülich GmbH, D-52425 Jülich, Germany and the §A. N. Belozersky Institute of Physico-Chemical Biology, Moscow State University, 119992 Moscow, Russia

Recoverin is a Ca^{2+}-regulated signal transduction modulator found in vertebrate retina that has been shown to undergo dramatic conformational changes upon Ca^{2+} binding to its two functional EF-hand motifs. To elucidate the differential impact of the N-terminal myristoylation as well as occupation of the two Ca^{2+} binding sites on recoverin structure and function, we have investigated a non-myristoylated E85Q mutant exhibiting virtually no Ca^{2+} binding to EF-2. Crystal structures of the mutant protein as well as the non-myristoylated wild-type have been determined. Although the non-myristoylated E85Q mutant does not display any functional activity, its three-dimensional structure in the presence of Ca^{2+} resembles the myristoylated wild-type with two Ca^{2+} but is quite dissimilar from the myristoylated E85Q mutant. We conclude that the N-terminal myristoyl modification significantly stabilizes the conformation of the Ca^{2+}-free protein (*i.e.* the T conformation) during the stepwise transition toward the fully Ca^{2+}-occupied state. On the basis of these observations, a refined model for the role of the myristoyl group as an intrinsic allosteric modulator is proposed.

Recoverin belongs to an ancient family of calcium-binding proteins termed the neuronal calcium sensor family (1, 2) and is mainly expressed in vertebrate photoreceptor cells (3, 4). The 23-kDa protein is composed of two domains, each of them harboring one non-functional and one functional EF-hand helix-loop-helix motif (5). Vertebrate photoreceptor cells respond to illumination by a decrease of the intracellular transmitters of excitation and adaptation, cGMP and Ca^{2+}, respectively. In the dark, at high Ca^{2+} concentration, the two functional EF-hands of recoverin (EF-2 and -3) are occupied by Ca^{2+} (6–8). In this state, recoverin is able to inhibit the G-protein-coupled receptor kinase GRK1[1] (rhodopsin kinase), thereby prolonging the lifetime of photoexcited rhodopsin (9–12). Upon illumination, decrease of cytoplasmic Ca^{2+} causes this inhibition to be relieved. This regulatory circuit is thought to be one out of several Ca^{2+}-dependent mechanisms that control adaptation of phototransduction to changing background light intensities (13, 14).

At its N terminus recoverin is heterogeneously acylated, the prevailing modification being a myristoyl chain (15). The observation of a Ca^{2+}-dependent partitioning of recoverin to membranes led to the proposal that it underwent a Ca^{2+}-myristoyl switch (16). The mechanics of this switch were unraveled by determining the solution structures of Ca^{2+}-free and Ca^{2+}-bound myristoylated recoverin via NMR spectroscopy. In the Ca^{2+}-free state of recoverin (T state) the myristoyl moiety is buried within a hydrophobic pocket, whereas in the Ca^{2+}-bound form (R state), the acyl group is extruded and thus available for interaction with other proteins or insertion into a lipid bilayer (17–19). Moreover, the myristoyl chain has been proposed to act as an intrinsic allosteric effector modifying the conformational equilibrium between T and R states (20).

Ca^{2+} binds to recoverin in a sequential fashion, *i.e.* occupation of high affinity EF-hand 3 is followed by filling of low affinity EF-hand 2. An intermediate state with Ca^{2+} bound solely to EF-3 can be prepared using myristoylated recoverin harboring the mutation E85Q, which virtually abolishes Ca^{2+} binding to EF-hand 2. Recently the three-dimensional structure of the myristoylated E85Q mutant was determined by NMR spectroscopy (21). It was shown to exhibit a hybrid fold with the N- and C-terminal domains resembling the corresponding portions of Ca^{2+}-free and Ca^{2+}-bound myristoylated wild-type recoverin, respectively. Consequently, the myristoyl group is still sequestered within a hydrophobic cavity and only partially unclamped. Biochemical studies on the myristoylated E85Q mutant confirmed that it can only bind one Ca^{2+} at saturating concentration (21, 22). Intriguingly, a fraction of myristoylated E85Q recoverin binds to membranes already at low free Ca^{2+} (2–9 μM), indicating that the presence of lipid bilayers may shift the conformational equilibrium toward a form of the E85Q mutant in which the myristoyl chain is exposed (22).

The presence of the N-terminal acyl group lowers the apparent Ca^{2+} affinity and adds cooperativity to the Ca^{2+} binding mode of recoverin (6). Because in the Ca^{2+}-saturated R state the myristoyl group is exposed to the solvent, the x-ray structure of non-myristoylated recoverin in the presence of Ca^{2+} has

* This work was supported by grants from the Deutsche Forschungsgemeinschaft (to K.-W. K.), a grant from the Forschungszentrum Jülich for visiting scientists (to I. I. S. and P. P. Ph.), the Ludwig Institute for Cancer Research (to P. P. Ph.), "International Projects" of Ministry of Industry and Science, Russian Federation (to P. P. Ph.), and the Russian Foundation for Basic Research (Grants 00-04-48332 and 00-04-48332). The costs of publication of this article were defrayed in part by the payment of page charges. This article must therefore be hereby marked "*advertisement*" in accordance with 18 U.S.C. Section 1734 solely to indicate this fact.

The atomic coordinates and structure factors (code 1OMR and 1OMV) have been deposited in the Protein Data Bank, Research Collaboratory for Structural Bioinformatics, Rutgers University, New Brunswick, NJ (http://www.rcsb.org/).

‖ To whom correspondence should be addressed. Tel.: 49-2461-61-3255; Fax: 49-2461-61-4216; E-mail: k.w.koch@fz-juelich.de.

[1] The abbreviations used are: GRK, G-protein-coupled receptor kinase; DTT, dithiothreitol; GCAP, guanylate cyclase activating protein; myr-, myristoylated; PMSF, phenylmethylsulfonyl fluoride; Rec, wild-type recoverin; Rec[E85Q], recoverin with E85Q substitution; Rec * 1 Ca, recoverin with Ca^{2+} bound to EF-3; Rec * 2 Ca, recoverin with Ca^{2+} bound to EF-2 and EF-3; ROS, rod outer segments; r.m.s., root mean square.

been suggested to represent a good approximation to the R form of the myristoylated protein (23, 24). We therefore speculate that the non-myristoylated E85Q mutant may represent a model of the myristoylated analog in the presence of membranes. Despite the lack of evidence for involvement of non-acylated recoverin in signal transduction, non-myristoylated forms of the protein are valuable models to delineate the pathways of Ca^{2+}-induced conformational changes.

In the present study we address the impact of the myristoyl group on the Ca^{2+}-dependent conformational transition in recoverin. To this end, we have determined the x-ray structure of the non-myristoylated E85Q mutant and compared it to the non-myristoylated wild-type as well as to the myristoylated mutant published recently (21). Furthermore, to gain more insight into the biochemical properties of the non-acylated E85Q variant, we investigated key functional parameters such as Ca^{2+} binding, association with hydrophobic matrices, and inhibition of rhodopsin kinase. Finally we asked how the biochemical properties of the E85Q mutant correlate with the structural information that we obtained on this mutant.

EXPERIMENTAL PROCEDURES

Preparation of Wild-type Recoverin, Mutant E85Q Recoverin, and Rhodopsin Kinase—Preparation of recombinant non-myristoylated forms of wild-type and mutant recoverin has been described previously (22). The purification of rhodopsin kinase was performed by a modification of a published procedure (25). Bovine rod outer segments (ROS, 100–200 mg of rhodopsin) were homogenized in low salt buffer (20 mM Tris-HCl, pH 7.5, 2 mM $MgCl_2$, 0.1 mM EDTA, 1 mM dithiothreitol (DTT), 1 mM phenylmethylsulfonyl fluoride (PMSF)), illuminated at 4 °C for 10 min by a 150-watt white light source, and then ROS membranes were pelleted. Rhodopsin kinase activity was extracted from ROS membranes by washing three times in 10–15 ml of high salt buffer (20 mM Tris-HCl, pH 7.5, 300 mM NaCl, 0.1 mM EDTA, 2 mM $MgCl_2$, 1 mM DTT, and 1 mM PMSF) in the dark. The combined extract containing rhodopsin kinase activity was diluted with salt-free buffer (5 mM Tris-HCl, pH 7.5, 0.1 mM EDTA, 2 mM $MgCl_2$, 3 mM DTT, and 1 mM PMSF) to a final concentration of 125 mM NaCl and was loaded onto a heparin-agarose column. After a washing step with two bed volumes of buffer (20 mM Tris-HCl, pH 7.5, 125 mM NaCl, 0.1 mM EDTA, 2 mM $MgCl_2$, 3 mM DTT, and 1 mM PMSF) rhodopsin kinase was eluted with a solution containing 20 mM Tris-HCl, pH 7.5, 280 mM NaCl, 0.1 mM EDTA, 2 mM $MgCl_2$, 3 mM DTT, and 1 mM PMSF. The fractions containing rhodopsin kinase activity were combined, diluted with salt-free buffer to yield 100 mM NaCl, and applied to a Mono-Q (5/5) column. Rhodopsin kinase activity was eluted with a linear gradient of 0–400 mM NaCl in 20 mM Tris-HCl, pH 7.5. All procedures were performed at 0–4 °C. The specific activity of purified rhodopsin kinase was 10–19 units/ml, with 1 unit being defined as the activity that catalyzes the incorporation of 1 nmol of ^{32}P per minute into light-activated rhodopsin (25).

$^{45}Ca^{2+}$ Binding Assay—Binding of $^{45}Ca^{2+}$ to wild-type recoverin and the E85Q mutant was investigated as described previously (21, 22). In summary, 50 or 100 μM protein was dissolved in 20 mM HEPES-KOH, pH 7.5, 100 mM NaCl, and 1 mM DTT and transferred to Centricon 10 devices (Amicon). Radioactive $^{45}CaCl_2$ was added, the samples were centrifuged for 1 min (7000 rpm, tabletop centrifuge Eppendorf model 5415), and radioactivity of the filtrate was counted (free Ca^{2+}). Next, non-radioactive $CaCl_2$ was added and the centrifugation procedure was repeated. Protein-bound Ca^{2+} *versus* free Ca^{2+} was determined from the excess Ca^{2+} in the protein sample over that present in the ultrafiltrate. Data were analyzed as described previously (22).

Phenyl-agarose Binding Assay—The phenyl-agarose binding assay was performed according to a published procedure (16). Briefly, 2 μM wild-type recoverin or mutant E85Q were mixed with 100 μl phenyl-agarose (Sigma) and incubated at 37 °C (Eppendorf thermomixer 5436, 1,000 rpm) for 15 min in 20 mM HEPES, pH 7.5, 150 mM NaCl, 20 mM $MgCl_2$, 1 mM DTT, 3 mM EGTA, and 0–50 mM $CaCl_2$ (total volume, 1000 μl). The mixture was centrifuged for 15 min (14,000 rpm, table-top centrifuge Eppendorf model 5415), and protein concentration in the supernatant was determined by a Bradford protein assay (Bio-Rad).

Rhodopsin Kinase Assay—The assay mixture in a final volume of 50 μl contained 10 μM rhodopsin (urea-washed ROS), 20 mM Tris-HCl, pH 7.5, 2 mM $MgCl_2$, 1 mM [γ-^{32}P]ATP (30–100 dpm/pmol), 1 mM DTT, 1 mM PMSF, and 0.3 unit of rhodopsin kinase. Where appropriate, wild-type recoverin or the E85Q mutant and a Ca^{2+}/bisaminobromophenoxyethane tetraacetate buffer were added (20). The reaction was initiated by addition of ATP, and samples were incubated in continuous light for 30 min at 37 °C. Incubation was terminated by adding 1 ml of 10% (w/v) trichloroacetic acid. The resulting precipitate was collected by centrifugation and washed 3–4 times with 1 ml of 10% trichloroacetic acid; the pellet was used for Cerenkov counting.

Recoverin Crystallization—Non-myristoylated recombinant bovine recoverin was crystallized using the hanging-drop setup in a buffer containing 100 mM Tris-HCl, pH 8.0, 1 mM $CaCl_2$, and 1 mM $MgCl_2$ with the reservoir solution additionally containing 70–80% saturated ammonium sulfate. Crystals measuring 150–250 μm in each dimension grew within 4–6 weeks under these conditions.

Data Collection—Crystallographic datasets were collected at 100 K. Because crystals could not be grown in the presence of cryoprotectants, they were soaked in reservoir solution containing 5, 10, and 15% (v/v) glycerol for 10 min each and 30% for 10 s prior to cryocooling.

Native data were recorded at beamline ID14-1 of the European Synchrotron Radiation Facility (Grenoble, France) tuned to a wavelength of 0.934 Å on an ADSC-Q4R detector (ADSC-Quantum). Data processing, including reflections up to 1.5- and 1.9-Å resolution for wild-type and mutant, respectively, was carried out using MOSFLM (26) and SCALA, the latter of which is part of the CCP4 software suite (27).

Structure Solution—Both recoverin structures were determined by molecular replacement using a single dataset each. The crystal structure of non-myristoylated recombinant bovine recoverin reported previously (23) was used as a starting model for refinement of the wild-type structure. Following preliminary refinement using the CNS software package (28), all regions poorly defined in electron density were removed from the model and re-established in an iterative process, including several cycles of positional refinement and manual rebuilding using the program O (29). To minimize model bias in the refinement process, electron density was modified using the DM package (CCP4), including solvent flattening, histogram mapping, and Sayre's equation. This finally allowed for portions of the structure not well-defined in $2F_o - F_c$ maps (*i.e.* residues 2–6 and 201–202) to be built as well. A total of 85 crystallographic water molecules could be determined in the structure.

The resulting improved wild-type recoverin model served as a starting point for determination of the E85Q mutant structure, which was performed using essentially the same strategy. In this case, residues 2–6, 75–77, and 198–202 could not be properly defined even by the use of density modification algorithms. The number of water molecules in this structure was 76. For statistics on data collection and refinement refer to Table I.

According to Ramachandran plots generated with PROCHECK (CCP4), both models exhibit good geometry with 98.4 and 100%, respectively, of the residues in the allowed regions. Exceptions in the wild-type structure include serines 4 and 6 located in the N-terminal tail poorly defined in the $2F_o - F_c$ map and aspartate 74, which is part of the Ca^{2+} binding EF-2 loop. Figures were generated using MOLSCRIPT (30) and RASTER3D (31) using secondary structure assignments as given by the DSSP program (32). Surface representations were prepared with VMD (33). For depicting solution structures determined by NMR spectroscopy the individual structure exhibiting the lowest r.m.s. deviation from the mean, as determined with MOLMOL (34), was selected from the ensemble. Calculation of EF-hand interhelical angles was performed using the program INTERHLX (obtained from nmr.uhnres.utoronto.ca/ikura/datasoft.html).

RESULTS

Ca^{2+} Binding Properties of Recoverin Variants—To assess the functional activity of non-myristoylated E85Q mutant recoverin, we first investigated its ability to bind radioactive $^{45}Ca^{2+}$ (Fig. 1). One Ca^{2+} ion is bound to the mutant protein with an apparent dissociation constant (K_D) of 0.26 μM, and binding is saturated above 10 μM. These observations are in agreement with data reported recently (K_D = 0.15 μM (21)). To assure our method worked properly, we repeated measurements on non-acylated wild-type recoverin as a control showing that it binds two Ca^{2+} non-cooperatively with an apparent K_D of 0.21 and 6.2 μM, respectively (Fig. 1). Our results confirmed previous observations indicating that EF-hand 3 is the high affinity Ca^{2+} binding site in recoverin, irrespective of the myristoylation state (6).

TABLE I
X-ray crystallographic data

$R_{meas} = \Sigma_h [N_h/(N_h - 1)]^{1/2} \Sigma_i |I_{i,h} - \langle I_h \rangle| / \Sigma_h \Sigma_i I_{i,h}$ according to Ref. 51, also termed redundancy-independent merging R factor ($R_{r.i.m.}$) with $I_{i,h}$ representing the ith out of N_h measurements and $\langle I_h \rangle$ the mean of all observations of I_h. For calculation R_{free}, 5% of all reflections were reserved.

	Recombinant bovine recoverin	
	Wild-type	E85Q mutant
Data collection		
Space group	I4	I4
Cell dimensions		
$a = b$, c (Å) (T = 100 K)	84.05, 59.18	84.33, 58.81
Resolution (Å)	1.50	1.90
Beamline	Grenoble ID14-1	Grenoble ID14-1
Detector	ADSC-Q4R	ADSC-Q4R
Wavelength (Å)	0.934	0.934
Unique reflections	33042	16253
Average multiplicity	3.8	3.8
Completeness (%)	99.9 (100.0)[a]	99.7 (100.0)[a]
R_{meas} (%)	6.8 (42.2)[a]	8.7 (20.8)[a]
$I/\sigma(I)$	5.2 (2.0)[a]	4.7 (3.1)[a]
Refinement		
Resolution (Å)	48.39-1.50	59.63-1.90
R_{work} (%)	24.9	24.0
R_{free} (%)	25.0	24.9
Residue range	2-202	7-74, 78-197
Number of atoms		
Protein	1638	1542
Water	85	76
Ca^{2+}	1	1
r.m.s. deviation		
Bonds (Å)	0.007	0.007
Angles (°)	1.329	1.383
E85Q *versus* wt (backbone r.m.s. deviation) (Å)	0.30	

[a] Numbers in parentheses indicate the value for the highest resolution shell.

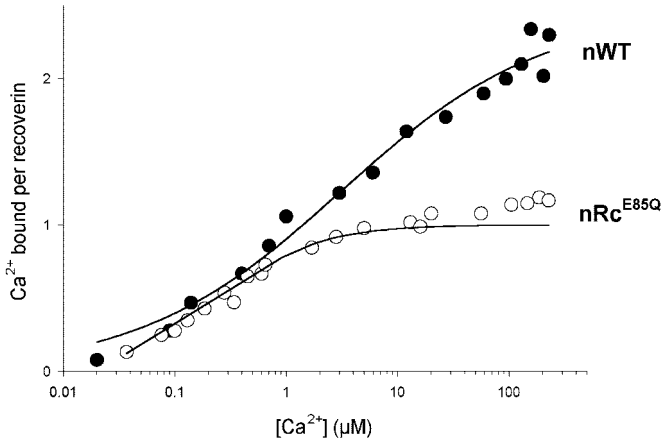

FIG. 1. **$^{45}Ca^{2+}$ binding to non-myristoylated forms of recoverin.** Wild-type recoverin (●) and the E85Q mutant (○) were incubated with increasing free Ca^{2+}. *Solid lines* represent the best fit to the two-site model (K_{D1} = 0.21 μM and K_{D2} = 6.2 μM for non-myristoylated wild-type recoverin) as described in ref. 6. Binding of $^{45}Ca^{2+}$ to the E85Q mutant yielded a K_D of 0.26 μM.

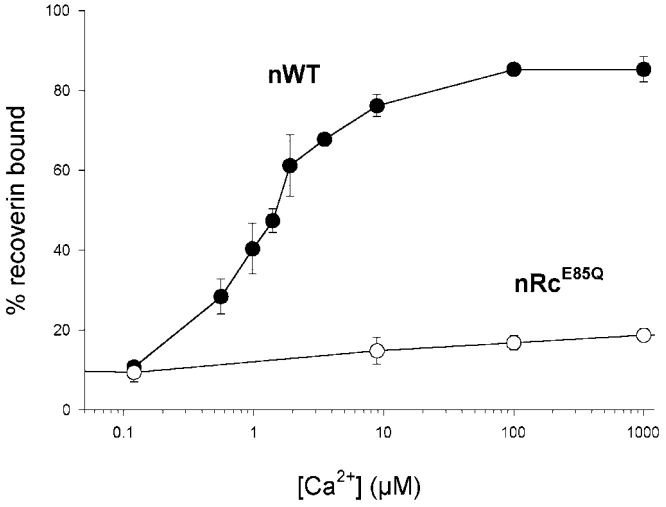

FIG. 2. **Binding of non-myristoylated wild-type recoverin (●) and the E85Q variant (○) to phenyl-agarose as a function of Ca^{2+} concentration.** Binding was half-maximal at 1.5 μM Ca^{2+} for the wild-type protein.

Interaction with Phenyl-agarose—Binding of recoverin to phenyl-agarose is thought to depend on the Ca^{2+}-induced exposure of hydrophobic residues and not on the presence of the myristoyl group (16). We applied this assay to test whether the non-myristoylated E85Q variant could bind to phenyl-agarose in a fashion similar to the wild-type (Fig. 2). In fact, the mutant protein did not display any binding activity at all. By contrast, wild-type recoverin included as a control bound to the hydrophobic matrix with half-saturation occurring at 1.5 μM Ca^{2+}.

Inhibition of Rhodopsin Kinase—One more characteristic feature of recoverin is its capability of inhibiting rhodopsin kinase in a Ca^{2+}-dependent manner (9–11, 35, 36). Myristoylation of recoverin is dispensable for this activity, because the non-acylated protein inhibits rhodopsin kinase in a manner very similar to the myristoylated form (37). Thus, it is suggested that calcium triggers exposure of an interaction site that mediates inhibition of GRK1 by recoverin and is different from its N-terminal myristoyl group. We tested whether the mutant could inhibit rhodopsin kinase in a Ca^{2+}-dependent manner. As shown in Fig. 3, the E85Q mutant was not capable of inhibiting GRK1 to a significant extent. In contrast, the non-myristoylated wild-type used as a positive control inhibited rhodopsin kinase as expected.

Crystal Structure of Wild-type Recoverin and the E85Q Mutant—For elucidating the role of the myristoyl modification as an intrinsic modulator of the Ca^{2+}-induced conformational transition in recoverin, structural studies on non-myristoylated analogs are particularly useful. As a first approach, to

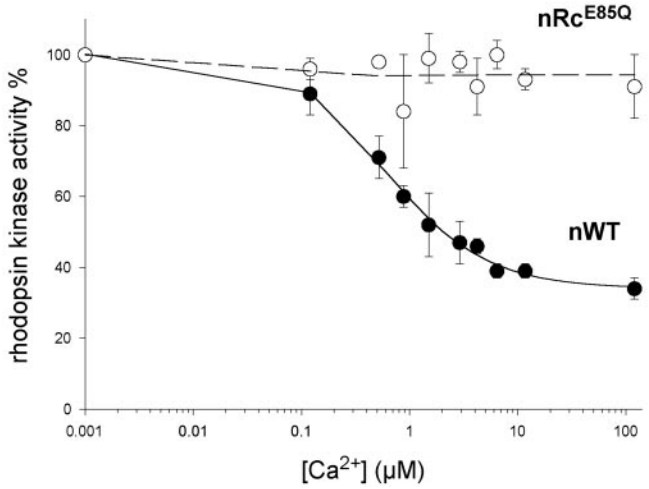

FIG. 3. **Inhibition of rhodopsin kinase by non-myristoylated forms of recoverin.** Phosphorylation of rhodopsin was measured as a function of free Ca^{2+} concentration in the presence of 30 μM non-myristoylated wild-type (●) and E85Q mutant recoverin (○). The *solid line* represents a fit according to the Hill model yielding the following values of IC_{50} (Ca^{2+}) and Hill coefficient n for non-myristoylated wild-type recoverin: IC_{50} = 0.6 μM, n = 0.96. No significant inhibition was observed in the presence of the E85Q variant.

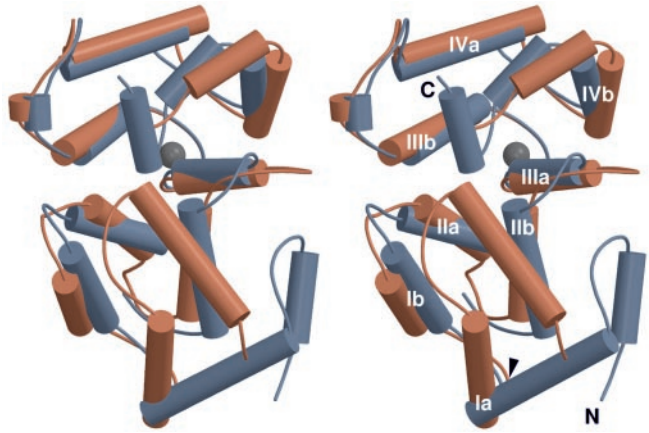

FIG. 4. **Stereo representation of the three-dimensional structure of myristoylated (*red* (21)) and non-myristoylated (*blue*; this study) E85Q mutant recoverin.** To highlight differences in the N-terminal domains, both structures have been aligned with respect to the C-terminal part (residues 100–185) resulting in a main-chain r.m.s. deviation of 1.99 Å for this region. EF-hands are labeled *I* through *IV* with *a* and *b* indicating the entering and exiting α-helices, respectively. Co-ordinates of the Ca^{2+} ion (*gray*) are taken from the structure of the non-myristoylated protein.

establish a positive control system, we have re-investigated the crystallographic structure of recombinant non-myristoylated bovine recoverin to a higher resolution (1.5 Å) than has been described previously (1.9 Å (23)). As a result, we were able to trace backbone and side-chain density in a larger portion of the molecule, particularly in the N- and C-terminal parts and the EF-2 loop. In the extreme termini (residues 2–6 and 201–202), use of conventional $2F_o - F_c$ and $F_o - F_c$ maps did not allow for satisfactory density allocation. However, based on density modification strategies, tentative coordinates are included for these stretches as well. The overall fold of the molecule is mostly identical to the published structure with a root mean square (r.m.s.) deviation of 0.45 Å for main-chain atoms and 1.03 Å for all non-hydrogen atoms. Likewise, the EF-2 Ca^{2+} binding site was found to be unoccupied despite the presence of 1 mM Ca^{2+} in the crystallization mother liquor. This is probably due to the high concentration of ammonium sulfate (approx. 3 M) in the

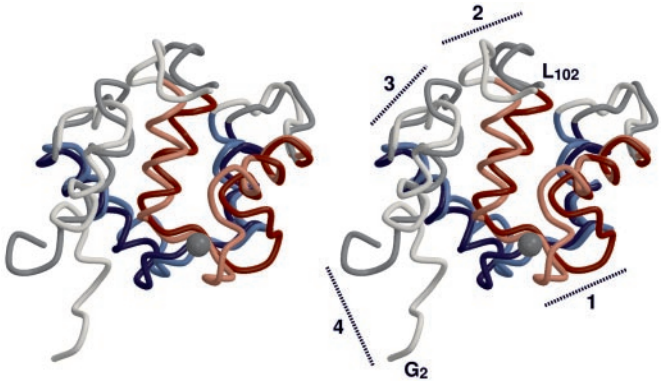

FIG. 5. **Stereo view of C_α traces of myristoylated recoverin with two Ca^{2+} (*lighter colors* (19)) and the non-myristoylated form with one Ca^{2+} (*darker colors*; this study).** Structures have been aligned with respect to the C-terminal domains (residues 100–185, main-chain r.m.s. deviation 1.86 Å), which have been omitted for clarity. EF-hands 1 and 2 are colored *blue* and *red*, respectively. Regions undergoing significant changes upon Ca^{2+} binding are indicated. See text for details.

solution, because it is well established that high ionic strength leads to electrostatic screening of ionic binding sites. Thus the Ca^{2+} activity is decreased into a range supporting binding to the high affinity EF-3 but not to the low affinity EF-2 site. Moreover, a model calculation of free Ca^{2+} in the presence of 3 M sulfate lead to an estimate well below 1 μM, which is clearly insufficient for Ca^{2+} binding to EF-2. The absence of Ca^{2+} in EF-2 in the crystal structures should therefore be viewed as a reflection of the ion concentrations in the samples and not an indication of an artifact due to crystal packing interactions. Although the non-liganded EF-2 loop is quite well defined in our crystal structure (mean atomic B factor 22.4 Å^2 for residues 72–82 compared with 21.7 Å^2 for the entire structure), we cannot exclude that it exhibits increased flexibility in solution.

Using crystallization conditions similar to those for the wild-type protein, crystals of the E85Q mutant diffracting to 1.9 Å were obtained. In this case, the entire polypeptide chain could be traced with the exception of residues 2–6, 75–77, and 198–202, which are poorly defined in electron density. The overall fold of the mutant protein turned out to be very similar to our wild-type structure with an r.m.s. deviation over the portions well-defined in both structures (residues 7–74 and 78–197) of 0.30 Å for main-chain atoms and 0.65 Å for all non-hydrogen atoms. This similarity is not surprising, because even the crystal structure of wild-type recoverin does not show any Ca^{2+} binding to EF-hand 2 (see above), which is disabled in the E85Q mutant. As has already been noted for the wild-type crystal structure, this fold is quite similar to the solution structure of the myristoylated protein with two Ca^{2+} bound (19). During the course of the present study, an NMR structure of the myristoylated E85Q mutant was published (21). Intriguingly, there are striking differences between the two structures of E85Q (Fig. 4).[2] In the myristoylated variant (shown in *red*), the conformation of the N-terminal domain is similar to the solution structure of the Ca^{2+}-free myristoylated wild-type protein, *i.e.* the T state (18), whereas in our non-myristoylated mutant (*blue*) it resembles the R state fold of the myristoylated wild-type with two Ca^{2+} (19). Specifically, the relatively limited

[2] Comparative structural representations included in this report display crystallographic structures along with NMR structures. We are aware of the possibility of artifacts, *e.g.* due to crystal packing interactions (38), that in certain cases may limit comparability of structures determined by different methods. However, due to the large extent of the majority of structural differences we refer to, we are confident that the conclusions drawn are nonetheless significant.

TABLE II
Selected interhelical angles in recoverin

Comparative overview showing interhelical angles in EF-hand motifs 1 through 4 as well as the inter-domain angles between the EF-2 exiting helix and the EF-3 entering helix (*italic*) for different recoverin structures. Angles were computed with INTERHLX using secondary structure assignments as given by the DSSP algorithm. *Boldface* indicates values for Ca^{2+}-occupied EF-hands. For NMR structures, values are given as mean ± S.D. of the entire ensemble.

	Non-myr. recoverin (x-ray)			Myr. recoverin (NMR)		
	Rec -1 Ca-	Rec[a] -1 Ca-	Rec[E85Q] -1 Ca-	Myr-Rec[b] -0 Ca-	Myr-Rec[E85Q][c] -1 Ca-	Myr-Rec[d] -2 Ca-
EF-1	108	108	108	170 ± 2	167 ± 3	115 ± 6
EF-2	130	129	130	136 ± 3	125 ± 3	**122 ± 6**
EF-3	**103**	**101**	**103**	119 ± 2	**87 ± 3**	**91 ± 4**
EF-4	103	99	103	99 ± 3	91 ± 5	88 ± 3
Inter-domain	*96*	*96*	*96*	*166 ± 2*	*109 ± 4*	*102 ± 4*

[a] Ref. 23; [b] Ref. 18; [c] Ref. 21; [d] Ref. 19.

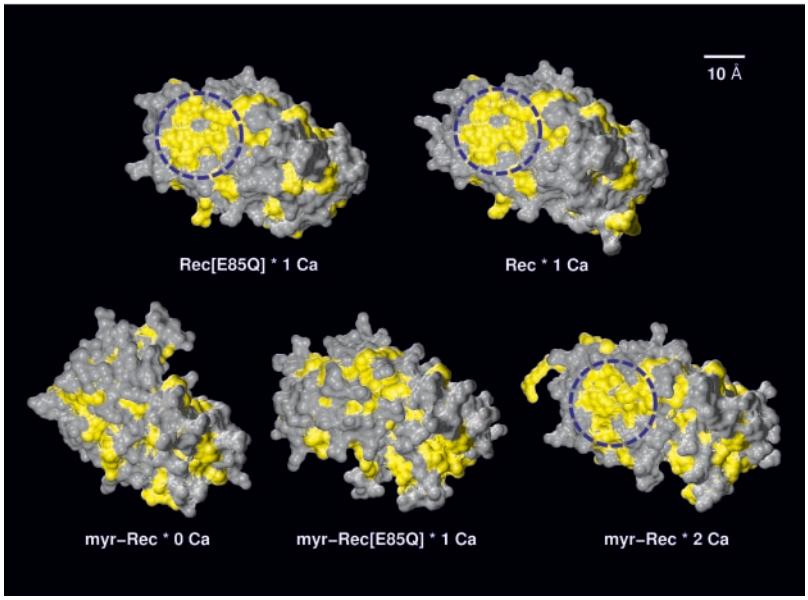

FIG. 6. **Hydrophobicity in solvent-accessible surfaces of different recoverin variants.** Apolar regions are highlighted in *yellow*. *Upper row*: non-myristoylated wild-type (*Rec*) and mutant (*Rec[E85Q]*) recoverin investigated in this study. *Bottom row*: myristoylated wild-type (*myr-Rec* (18, 19)) and mutant (*myr-Rec[E85Q]* (21)) variants. The number of Ca^{2+} ions bound to each protein is indicated. The *blue circle* marks a hydrophobic patch exposed in some of the structures. See text for details.

conformational changes in the C-terminal domain as well as rotation of the two domains with respect to each other near Gly^{96}, both of which are believed to be induced by Ca^{2+} binding to EF-3, are common to both structures. In contrast, rotation around Gly^{42} (indicated by an *arrowhead* in Fig. 4), leading to a considerable displacement of the N-terminal α-helix and the entering helix of EF-1, is only observed in the non-acylated mutant. These observations suggest that the unmodified protein possesses the intrinsic capability of undergoing almost the entire Ca^{2+}-induced conformational transition upon Ca^{2+} binding to EF-3, whereas in the myristoylated form the N-terminal domain is locked in the T state until Ca^{2+} is bound to EF-2.

Because in Ca^{2+}-saturated recoverin the myristoyl group is extruded and does not significantly interact with the protein moiety (19), we decided to use the NMR structure of the myristoylated protein with two Ca^{2+} as a model for the corresponding non-myristoylated analog. Although this is a reasonable assumption, equivalence of tertiary folds cannot be unequivocally proven in the absence of a structure of Ca^{2+}-saturated non-myristoylated recoverin. This stated, the differences between our crystallographic structure of non-myristoylated recoverin with one Ca^{2+} and the solution structure of the myristoylated protein with two Ca^{2+} should be mainly related to Ca^{2+} binding to EF-2. The most significant structural alterations are highlighted in Fig. 5. Establishment of the Ca^{2+} co-ordination sphere requires "flipping" of the Ca^{2+}-binding loop (residues 72–82, region 1), which is associated with a decrease in the EF-2 interhelical angle (Table II, below). The resulting movement of the domain linker (residues 95–101, region 2) by ~5 Å causes a steric clash with a stretch of residues connecting the N-terminal α-helix to the entering helix of EF-1 (residues 18–24, region 3), which forces a concerted movement of this loop. Consequently, the orientation of the N-terminal helix (region 4) also changes considerably. Comparison of these two recoverin structures thus enables us to trace structural implications of Ca^{2+} binding to EF-2 throughout the entire domain. Moreover, as the structure of the non-acylated E85Q mutant is virtually identical to the non-acylated wild-type, both of which contain one Ca^{2+} bound to EF-3, these effects of EF-2 occupation probably account for the functional inactivity of the mutant, as discussed below.

The interhelical angle defined by the entering and exiting helices is a sensitive indicator of conformational changes in EF-hand modules (39). Table II gives a compilation of this parameter for EF-hands 1 through 4 for all recoverin structures currently available. The angle defined by the exiting helix of EF-2 and the entering helix of EF-3 has been included for monitoring the arrangement of the N-terminal domain relative to the C-terminal portion. The values listed support our conclusion that, upon occupation of EF-3 in the non-myristoylated protein, EF-1 adopts a configuration reminiscent of the sterical arrangement in myristoylated recoverin with two Ca^{2+}. At the same time, the interhelical angle in EF-2 is similar to the value in the myristoylated E85Q mutant and is thus representative of a non-liganded EF-2 in the T/R intermediate state. The difference in EF-2 interhelical angle between these structures on the one hand and the Ca^{2+}-free protein on the other may

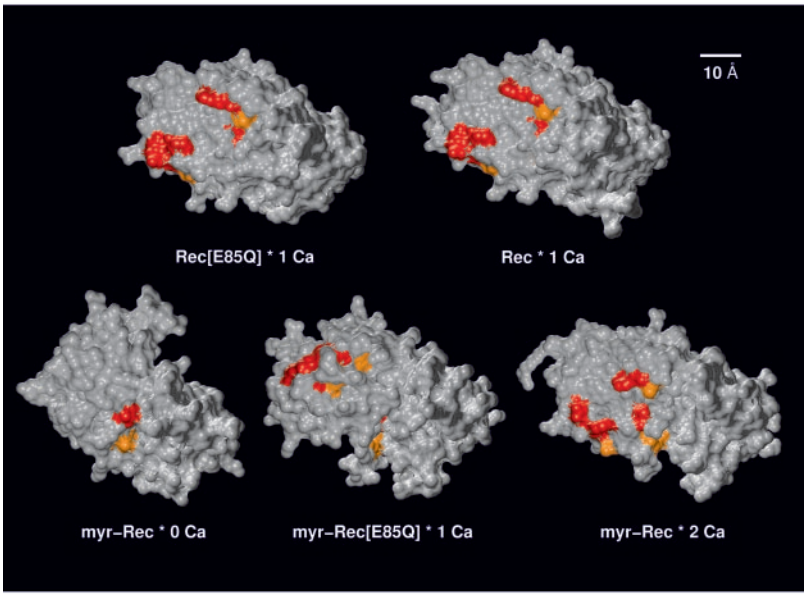

FIG. 7. **Arrangement of side chains critical for interaction with rhodopsin kinase (as defined in Ref. 41).** Residues probably involved in the binding interface according to these authors are colored in *red*, those of minor significance in *orange*. Abbreviations are as in Fig. 6.

indicate a slight conformational change in EF-2, which is associated with Ca^{2+} binding to EF-3 and the resulting re-arrangement of the domain interface. With respect to the C-terminal domain, interpretation of the results is more complicated. For example, the angle of EF-3 in the crystal structures containing one Ca^{2+}, although clearly different from the unoccupied EF-3 in Ca^{2+}-free myristoylated recoverin, is still not identical to the myristoylated structures with one or two Ca^{2+} ions. Moreover, the extent of the rotation around Gly^{96} in non-myristoylated E85Q recoverin, which ultimately results from Ca^{2+} binding to EF-3, is more similar to the myristoylated protein with two Ca^{2+} than to the myristoylated E85Q mutant with one Ca^{2+}. These observations indicate that the increased conformational rigidity of the N-terminal domain in the presence of the buried myristoyl group on the one hand limits the magnitude of the domain rotation but on the other hand in some way facilitates the Ca^{2+}-induced "opening" movement of EF-3. Thus, the bidirectional transfer of conformational information across the domain interface is significantly modulated by the presence of the N-terminal myristoyl moiety.

DISCUSSION

The three-dimensional structure of non-myristoylated recombinant bovine recoverin has been determined by x-ray crystallography almost a decade ago (23). In the meantime, solution structures of the myristoylated protein in the Ca^{2+}-free state (18) as well as with Ca^{2+} bound to EF hands 2 and 3 (19) have been published. These data revealed that binding of Ca^{2+} essentially modifies the equilibrium between two dramatically different conformational states commonly referred to as the T and R state. This transition includes two major rotational components among glycine residues at positions 42 and 96. Recently, Ames *et al.* (21) described the structure of the myristoylated E85Q mutant determined by NMR spectroscopy in the presence of 1 mM Ca^{2+}. They found the protein to exhibit a hybrid structure with the N- and C-terminal domains adopting an overall fold resembling the corresponding portions of Ca^{2+}-free and Ca^{2+}-bound myristoylated recoverin, respectively. Although these studies allowed for the different conformational states of acylated recoverin to be described in detail, the precise role of the N-terminal myristoyl modification in the context of the Ca^{2+}-induced conformational transition has remained unclear.

In this study, we have determined the crystallographic structure of non-myristoylated recoverin bearing the E85Q substitution which virtually abolishes Ca^{2+} binding to EF-hand 2. An improved structure of the wild-type protein at 1.5-Å resolution allowed us to trace larger portions of the molecule than was previously possible. The overall fold of the wild-type and mutant recoverin is almost identical, which can be explained by the absence of Ca^{2+} binding to EF-2 even in the wild-type under the crystallization conditions employed. Thus, in both cases the protein is trapped in an intermediate state reflecting conformational changes induced by Ca^{2+} binding to EF-3. Several conclusions can be drawn from the intriguing similarity between these two structures and the solution structure of the fully Ca^{2+}-occupied myristoylated protein.

First, the Ca^{2+}-induced conformational transition initially

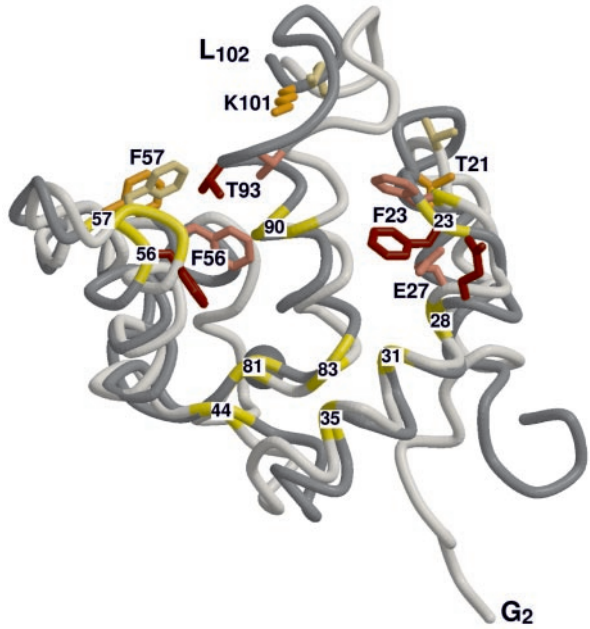

FIG. 8. **C_α trace superposition (identical to Fig. 5 with ~180° rotation) of non-myristoylated recoverin with one Ca^{2+} (*darker colors*) and myristoylated recoverin with two Ca^{2+} (*lighter colors*) showing positional re-arrangement of hydrophobic residues forming the patch defined in Fig. 6 (*yellow backbone*) and of side chains probably (*light* and *dark red*) and possibly (*light* and *dark orange*) involved in rhodopsin kinase inhibition (see Fig. 7).**

observed in the NMR structures of myristoylated recoverin appear for the most part not to require Ca^{2+} binding to EF-2 in the non-myristoylated protein. Instead, upon Ca^{2+} binding to EF-3 both domains adopt a characteristic R state fold, including rotational movements about Gly^{42} and Gly^{96} (Fig. 4). This conclusion relies on the assumption that in the Ca^{2+}-free state recoverin structure is largely independent of the myristoylation state. Unfortunately, structural information on non-acylated Ca^{2+}-free recoverin is currently unavailable. Nonetheless, there are several lines of indirect evidence supporting this view. Dizhoor *et al.* (20) have analyzed the susceptibility of acylated and non-acylated recoverin to tryptic cleavage in the presence and absence of Ca^{2+}. They found Ca^{2+} to increase resistance toward degradation, this effect being even more pronounced with the non-acylated protein. In a CD-spectroscopic study performed by Kataoka *et al.* (40), the Ca^{2+}-induced increase in ellipticity at $\lambda = 208$ nm and $\lambda = 222$ nm was reported to be independent of the myristoylation state. Finally, binding of the fluorescent dye 1-anilinonaphthalene-8-sulfonate by recoverin increases dramatically upon Ca^{2+} binding in both the myristoylated and the non-myristoylated state (41). These data indicate that the Ca^{2+}-induced conformational changes in unmodified recoverin are at least comparable to those observed for the native acylated protein. Of course, we cannot exclude the possibility that the presence of the myristoyl moiety may induce minor structural changes in the Ca^{2+}-free protein, the NMR structure of which has revealed a tight interaction of the acyl chain with its hydrophobic pocket. Indeed, when comparing deuterium exchange rates of myristoylated and non-myristoylated recoverin in the presence and absence of Ca^{2+}, Neubert *et al.* (42) found the myristoylation state to affect isotope exchange in certain recoverin fragments, although for both the myristoylated and the non-myristoylated protein, significant effects of Ca^{2+} binding were observed. Attempts to crystallize Ca^{2+}-free non-myristoylated recoverin have thus far been unsuccessful.

A second conclusion from our data concerns the role of the myristoyl group. As stated above, the conformational changes in the C-terminal domain induced by occupancy of EF-3 and the subsequent reorganization at the domain interface tend to destabilize the T state in the N-terminal part even in the absence of Ca^{2+} binding to EF-2. This effect is counterbalanced in the presence of the myristoyl moiety, which is able to stabilize the arrangement of the N-terminal domain in the Ca^{2+}-free state. As a result, in the myristoylated protein binding of Ca^{2+} to EF-2 is essential to shift the conformational equilibrium toward the R state. In this model, Ca^{2+} binding to EF-2 would not directly drive the rotation about Gly^{42}, resulting in the N terminus "pulling" the myristoyl group out of its hydrophobic pocket, as previously suggested, but is likely to destabilize the hydrophobic interactions of the myristoyl with its environment, rendering the buried state thermodynamically less favorable. This would ultimately allow the intrinsic tension of the domain to be relieved, partly by means of the aforementioned rotation.

In the absence of the myristoyl modification, the structural impact of Ca^{2+} binding to EF-2 is greatly reduced (Fig. 5). Nonetheless, it is absolutely required to attain the R state, because the E85Q mutant neither displays binding to phenyl-agarose (Fig. 2) nor is able to inhibit rhodopsin kinase (Fig. 3).

A thorough comparison of available recoverin structures offers possible explanations for this behavior. Fig. 6 illustrates the pattern of polarity on the solvent-accessible surface computed for various recoverin structures. Upon Ca^{2+} binding, the myristoylated protein exposes a large hydrophobic patch (*blue circle*), which is made up of aromatic (Phe^{23}, Trp^{31}, Phe^{35}, Phe^{56}, Phe^{57}, Phe^{83}) and aliphatic (Leu^{28}, Ile^{44}, Leu^{81}, Leu^{90}) side chains and is surrounded by charged and polar residues. Although not discernible in the myristoylated E85Q mutant, in the non-myristoylated structures this patch is formed in its general outline, but the pattern still changes further in the fully Ca^{2+}-occupied protein. Specifically, the terminal hydroxyl oxygen of Tyr^{86}, which is located in the center of the hydrophobic patch and is readily solvent-accessible in non-myristoylated recoverin with one Ca^{2+}, becomes almost completely buried upon Ca^{2+} incorporation into EF-2. Because this hydrophobic region is a good candidate for mediating the Ca^{2+}-induced binding of recoverin to phenyl-agarose, these observations may explain why the E85Q mutant (largely irrespective of myristoylation) does not efficiently bind to this hydrophobic matrix in the presence of Ca^{2+}.

A similar approach was used to understand the different capabilities of the same recoverin variants to inhibit rhodopsin kinase in a Ca^{2+}-dependent manner. In a recent mutational study on the frog recoverin homolog S-modulin, Tachibanaki *et al.* (43) identified seven conserved amino acid residues that were proposed to constitute an interaction surface for rhodopsin kinase. Based on the degree of preservation of Ca^{2+}-induced conformational changes as assessed by CD spectroscopy, the authors defined "probable" (residues Phe^{23}, Glu^{27}, Phe^{56}, and Thr^{93}) and "possible" (residues Thr^{21}, Phe^{57}, and Lys^{101}) interaction sites. In Fig. 7 these groups of residues (colored *red* and *orange*, respectively) are mapped to the solvent-accessible surface in the recoverin structures under consideration. It is evident that these crucial side chains localize near each other only upon Ca^{2+} binding to EF-2 and EF-3 in the myristoylated protein. The conformational transition, which is allowed in the acylated E85Q mutant upon EF-3 occupation, does not establish the interaction surface, and even the non-acylated wild-type and mutant proteins containing one Ca^{2+}, while displaying an overall fold resembling the native R state, do not present the same sterical arrangement of these critical residues. Fig. 8 emphasizes individual side-chain displacements occurring in the N-terminal domain of non-myristoylated recoverin upon binding of Ca^{2+} to EF-2 and thus accounting for the differences in surface properties between *Rec * 1 Ca* and *myr-Rec * 2 Ca* shown in Figs. 6 and 7.

The three-dimensional structures of several other members of the neuronal calcium sensor family have been determined thus far. These include GCAP-2 (44), neurocalcin (45), human (46), and yeast frequenin (47). Although the overall topology of their folds resembles the structure of recoverin, they also differ in several aspects. For example, an attached myristoyl group can adopt diverse functions, and although some proteins such as recoverin, hippocalcin, and neurocalcin δ exhibit a Ca^{2+}-myristoyl switch, others like GCAP-1, GCAP-2, and frequenin apparently do not (48–50). Diversity of Ca^{2+} signaling via neuronal calcium sensor proteins is also mirrored by the variety of target proteins, including various kinases, membrane-bound guanylate cyclases, adenylate cyclases, ion channels, and cytoskeletal proteins. Our results indicate that subtle changes in surface properties can dramatically alter the biochemical characteristics of recoverin, such as interaction with phenyl-agarose and rhodopsin kinase inhibition. In line with these conclusions, minor differences in surface exposition of amino acid side chains might well account for the diversity of neuronal calcium sensor signaling.

Acknowledgments—We thank Dr. Jörg Labahn for helpful discussion. Furthermore, support by the technical staff at Beamline ID14-1, ESRF (Grenoble, France) is acknowledged.

REFERENCES

1. Braunewell, K. H., and Gundelfinger, E. D. (1999) *Cell Tissue Res.* **295,** 1–12
2. Burgoyne, R. D., and Weiss, J. L. (2001) *Biochem. J.* **353,** 1–12

3. Dizhoor, A. M., Ray, S., Kumar, S., Niemi, G., Spencer, M., Brolley, D., Walsh, K. A., Philipov, P. P., Hurley, J. B., and Stryer, L. (1991) *Science* **251,** 915–918
4. Lambrecht, H. G., and Koch, K. W. (1991) *EMBO J.* **10,** 793–798
5. Kawasaki, H., Nakayama, S., and Kretsinger, R. H. (1998) *Biometals* **11,** 277–295
6. Ames, J. B., Porumb, T., Tanaka, T., Ikura, M., and Stryer, L. (1995) *J. Biol. Chem.* **270,** 4526–4533
7. Matsuda, S., Hisatomi, O., and Tokunaga, F. (1999) *Biochemistry* **38,** 1310–1315
8. Permyakov, S. E., Cherskaya, A. M., Senin, I. I., Zargarov, A. A., Shulga-Morskoy, S. V., Alekseev, A. M., Zinchenko, D. V., Lipkin, V. M., Philippov, P. P., Uversky, V. N., and Permyakov, E. A. (2000) *Protein Eng.* **13,** 783–790
9. Kawamura, S., Hisatomi, O., Kayada, S., Tokunaga, F., and Kuo, C. H. (1993) *J. Biol. Chem.* **268,** 14579–14582
10. Chen, C.-K., Inglese, J., Lefkowitz, R. J., and Hurley, J. B. (1995) *J. Biol. Chem.* **270,** 18060–18066
11. Klenchin, V. A., Calvert, P. D., and Bownds, M. D. (1995) *J. Biol. Chem.* **270,** 16147–16152
12. Erickson, M. A., Lagnado, L., Zozulya, S., Neubert, T. A., Stryer, L., and Baylor, D. A. (1998) *Proc. Natl. Acad. Sci. U. S. A.* **95,** 6474–6479
13. Pugh, E. N., Jr., Nikonov, S., and Lamb, T. D. (1999) *Curr. Opin. Neurobiol.* **9,** 410–418
14. Burns, M. E., and Baylor, D. A. (2001) *Annu. Rev. Neurosci.* **24,** 779–805
15. Dizhoor, A. M., Ericsson, L. H., Johnson, R. S., Kumar, S., Olshevskaya, E., Zozulya, S., Neubert, T. A., Stryer, L., Hurley, J. B., and Walsh, K. A. (1992) *J. Biol. Chem.* **267,** 16033–16036
16. Zozulya, S., and Stryer, L. (1992) *Proc. Natl. Acad. Sci. U. S. A.* **89,** 11569–11573
17. Ames, J. B., Tanaka, T., Ikura, M., and Stryer, L. (1995) *J. Biol. Chem.* **270,** 30909–30913
18. Tanaka, T., Ames, J. B., Harvey, T. S., Stryer, L., and Ikura, M. (1995) *Nature* **376,** 444–447
19. Ames, J. B., Ishima, R., Tanaka, T., Gordon, J. I., Stryer, L., and Ikura, M. (1997) *Nature* **389,** 198–202
20. Dizhoor, A. M., Chen, C. K., Olshevskaya, E., Sinelnikova, V. V., Phillipov, P., and Hurley, J. B. (1993) *Science* **259,** 829–832
21. Ames, J. B., Hamasaki, N., and Molchanova, T. (2002) *Biochemistry* **41,** 5776–5787
22. Senin, I. I., Fischer, T., Komolov, K. E., Zinchenko, D. V., Philippov, P. P., and Koch, K.-W. (2002) *J. Biol. Chem.* **277,** 50365–50372
23. Flaherty, K. M., Zozulya, S., Stryer, L., and McKay, D. B. (1993) *Cell* **75,** 709–716
24. Ames, J. B., Tanaka, T., Stryer, L., and Ikura, M. (1996) *Curr. Opin. Struct. Biol.* **6,** 432–438
25. Dean, K. R., and Akhtar, M. (1996) *Biochemistry* **35,** 6164–6172
26. Leslie, A. G. W. (1992) *Joint CCP4 + ESF-EAMCB Newsletter on Protein Crystallography*, No. 26
27. Collaborative computational project, n. 4. (1994) *Acta Crystallogr. Sect. D Biol. Crystallogr.* **50,** 760–763
28. Brunger, A. T., Adams, P. D., Clore, G. M., Delano, W. L., Gros, P., Grosse-Kunstleve, R. W., Jiang, J.-S., Kuszewski, J., Nilges, N., Pannu, N. S., Read, R. J., Rice, L. M., Simonson, T., and Warren, G. L. (1998) *Acta Crystallogr. Sect. D Biol. Crystallogr.* **54,** 905–921
29. Jones, T. A., Zou, J.-Y., Cowan, S. W., and Kjeldgaard, M. (1991) *Acta Crystallogr. Sect. A* **47,** 110–119
30. Kraulis, P. J. (1991) *J. Appl. Crystallogr.* **24,** 946–950
31. Merritt, E. A., and Bacon, D. J. (1997) *Methods Enzymol.* **277,** 505–524
32. Kabsch, W., and Sander, C. (1983) *Biopolymers* **22,** 2577–2637
33. Humphrey, W., Dalke, A., and Schulten, K. (1996) *J. Mol. Graphics* **14,** 33–38
34. Koradi, R., Billeter, M., and Wüthrich, K. (1996) *J. Mol. Graphics* **14,** 51–55
35. Gorodovikova, E. N., Gimelbrant, A. A., Senin, I. I., and Philippov, P. P. (1994) *FEBS Lett.* **349,** 187–190
36. Gorodovikova, E. N., Senin, I. I., and Philippov, P. P. (1994) *FEBS Lett.* **353,** 171–172
37. Senin, I. I., Zargarov, A. A., Alekseev, A. M., Gorodovikova, E. N., Lipkin, V. M., and Philippov, P. P. (1995) *FEBS Lett.* **376,** 87–90
38. Srivastava, D. K., and Bernhard, S. A. (1987) *Annu. Rev. Biophys. Biophys. Chem.* **16,** 175–204
39. Yap, K. L., Ames, J. B., Swindells, M. B., and Ikura, M. (1999) *Proteins* **37,** 499–507
40. Kataoka, M., Mihara, K., and Tokunaga, F. (1993) *J. Biochem.* (*Tokyo*) **114,** 535–540
41. Hughes, R. E., Brzovic, P. S., Klevit, R. E., and Hurley, J. B. (1995) *Biochemistry* **34,** 11410–11416
42. Neubert, T. A., Walsh, K. A., Hurley, J. B., and Johnson, R. S. (1997) *Protein Sci.* **6,** 843–850
43. Tachibanaki, S., Nanda, K., Sasaki, K., Ozaki, K., and Kawamura, S. (2000) *J. Biol. Chem.* **275,** 3313–3319
44. Ames, J. B., Dizhoor, A. M., Ikura, M., Palczewski, K., and Stryer, L. (1999) *J. Biol. Chem.* **274,** 19329–19337
45. Vijay-Kumar, S., and Kumar, V. D. (1999) *Nat. Struct. Biol.* **6,** 80–88
46. Bourne, Y., Dannenberg, J., Pollmann, V., Marchot, P., and Pongs, O. (2001) *J. Biol. Chem.* **276,** 11949–11955
47. Ames, J. B., Hendricks, K. B., Strahl, T., Huttner, I. G., Hamasaki, N., and Thorner, J. (2000) *Biochemistry* **39,** 12149–12161
48. Olshevskaya, E. V., Hughes, R. E., Hurley, J. B., and Dizhoor, A. M. (1997) *J. Biol. Chem.* **272,** 14327–14333
49. O'Callaghan, D. W., Ivings, L., Weiss, J. L., Ashby, M. C., Tepikin, A. V., and Burgoyne, R. D. (2002) *J. Biol. Chem.* **277,** 14227–14237
50. Hwang, J. Y., and Koch, K. W. (2002) *Biochemistry* **41,** 13021–13028
51. Diederichs, K., and Karplus, P. A. (1997) *Nat. Struct. Biol.* **4,** 269–275